CrystEngComm

Accepted Manuscript

ROYAL SOCIETY OF CHEMISTRY

www.rsc.org/crystengcomm

Solvent-mediated assembly of chiral/achiral hydrophilic Ca(II)–tetrafluoroterephthalate coordination frameworks: 3D chiral water aggregation, structural transformation and selective CO_2 adsorption

Sheng-Chun Chen,[ab] Feng Tian,[a] Kun-Lin Huang,*[c] Cheng-Peng Li,[d] Jing Zhong,[a] Ming-Yang He,[ab] Zhi-Hui Zhang,[a] Hong-Ning Wang,[a] Miao Du*[d] and Qun Chen*[ab]

Received (in XXX, XXX) Xth XXXXXXXXX 200X, Accepted Xth XXXXXXXXX 200X
First published on the web Xth XXXXXXXXX 200X
DOI: 10.1039/b000000x

The spontaneous self-assembly reactions of 2,3,5,6-tetrafluoro-benzenedicarboxylic acid (H_2BDC-F_4) with $Ca(NO_3)\cdot 6H_2O$ in different solvents give rise to the generation of hydrophilic 3D chiral and achiral Ca(II)-organic frameworks $\{[Ca_4(BDC\text{-}F_4)_4(H_2O)_4]\cdot 4H_2O\}_n$ (**1**) and $[Ca(BDC\text{-}F_4)(MeOH)_2]_n$ (**2**), respectively. Complex **1** exhibits higher water solubility compared to **2**, and further dissolution of **1** in water results in a new achiral crystal $[Ca(BDC\text{-}F_4)(H_2O)_4]_n$ (**3**). All complexes have been characterized by elemental analysis, IR spectroscopy, single crystal and powder X-ray diffraction techniques. Complex **1** crystallizes in the tetragonal $P4_12_12$ chiral space group and features a rare binodal 5-connected network, directing by a unique 3D chiral (10,3)-*a* water aggregation consisting of two distinct helical arrays. Complex **2** crystallizes in the space group $C2/c$ and has a binodal 4-connected **pts** net. Complex **3** crystallizes in the space group $P2_1/m$ and presents a 2D layer framework containing the unprecedented polymeric $[Ca^{II}–H_2O]_n$ chain based on triple μ_2-O aqua bridiges. The structural discrepancies illustrate the solvent-induced effect on the construction and structural transformation of chiral and achiral coordination frameworks. Moreover, gas (N_2 and CO_2) adsorption studies on the dehydrated framework **1a** exhibit excellent selective CO_2 gas uptake at 195 K.

Introduction

Metal–organic frameworks (MOFs) have been considered as a promising class of porous crystalline materials with potential applications in gas sorption / separation, catalysis, magnetism, and photoluminescence.[1] The main advantage of MOFs over traditional porous materials is their highly designable nature, which allows the pore size, shape and even inner surface to be adjusted. The versatile pore features of MOFs, such as Lewis acidity, basicity, hydrophilicity, and chirality can be modified, relying on the combination of organic ligands and metal ions.[2] Thus, porous MOFs bearing different functional groups in the channels or voids have also been envisioned as ideal hosts for capturing various guests and also affecting their distributions, which may lead to a precise control of the stereoregularity of the resulting lattices. In this connection, MOFs with helical or chiral nature on the pore surfaces are of special interest.[3] For instance, Banerjee *et al.* have recently constructed a series of chiral MOFs with halogen-substituting ligands, which contain continuous helical water chains within the pores.[4] However, the investigation on chiral induction effect of guest species on MOFs is still a great challenge.

Thus far, a variety of structurally definite water aggregates, such as discrete water clusters,[5] and infinite 1D chains,[6] 2D layers,[7] or 3D water networks[8] have been observed in diverse crystalline hosts. Very recently, Wu *et al.* have reported the first example of chiral metallocycle templating of a 3D chiral zeolite-like water network comprising uniform *P* helical water chains.[9] Indeed, helical water motifs are broadly attractive for their fundamental importance in biological processes related to water and ion transport.[10] A practical approach to organize helical water chains is to employ chiral organic synthons or achiral multifunctional ligands with rich H-bonding groups.[11] In this respect, halogenated compounds are of particular interest as the noncovalent hydrogen and halogen bonds may improve the probability for creating supramolecular water helix.[4,12]

In our efforts to explore perfluorinated MOF materials,[13] we have illustrated the fluorine-induced coordination assembly of chiral networks by a flexible achiral Schiff base, where helical water chains play a key role.[13b] In this contribution, herein, we initiate the realization of chiral discrepancy with solvent-regulation assembly of two 3D Ca^{II} MOFs: chiral $\{[Ca_4(BDC\text{-}F_4)_4(H_2O)_4]\cdot 4H_2O\}_n$ (**1**) and achiral $[Ca(BDC\text{-}F_4)(MeOH)_2]_n$ (**2**) constructed from a rigid achiral tetrafluoroterephthalic acid (H_2BDC-F_4) in different solvent media. Remarkably, the unusual 5-connected coordination framework of **1** encapsulates a unique 3D chiral water network constructed from two distinct helical arrays, while **2** displays a binodal 4-connected **pts** network. Moreover, compared to **2**, **1** is highly water-soluble, and further evaporation of **1** in water results in an achiral 2D MOF $[Ca(BDC\text{-}F_4)(H_2O)_4]_n$ (**3**), revealing the water-induced structural transformation from chirality to achirality. In addition, the dehydrated framework **1a** exhibits a high gas adsorption selectivity of CO_2 over N_2 at 195 K.

Experimental

Materials and general methods

All reagents and solvents for synthesis and analysis were commercially available and used as received. The Fourier transform (FT) IR spectra (KBr pellets) were recorded on a Nicolet ESP 460 FT-IR spectrometer. Elemental analyses of carbon, hydrogen and nitrogen were performed on a PE-2400II (Perkin-Elmer) analyzer. Powder X-ray diffraction (PXRD) patterns were recorded on a Rigaku D/Max-2500 diffractometer at 40 kV and 100 mA for a Cu-target tube (λ = 1.5406 Å). The calculated PXRD patterns were obtained from the single-crystal diffraction data using the PLATON software.[14] Thermogravimetric analysis (TGA) experiments were carried out on a Dupont thermal analyzer from room temperature to 800 °C at a heating rate of 10 °C min^{-1} under nitrogen stream. The molar electrical conductivity was obtained in 10^{-3} M aqueous solution at 25 °C, with Radelkis OK 102/1 Conductometer.

Syntheses of complexes 1–3

{[Ca_4(BDC-F_4)$_4$(H_2O)$_4$]·4H_2O}$_n$ (1). An ethanol solution (6 mL) of H_2BDC-F_4 (71.4 mg, 0.3 mmol) was added to a DMF/ethanol solution (12 mL/6 mL) of $Ca(NO_3)_2·4H_2O$ (70.8 mg, 0.3 mmol) in a beaker. After *ca.* 30 min of stirring, the colorless solution was filtered and left to stand at room temperature. After seven weeks, colorless needle-like crystals of **1** suitable for X-ray diffraction were obtained by slow evaporation of the solvents in 62% yield (58.1 mg, based on H_2BDC-F_4). Anal. Calcd. for $C_8H_4CaF_4O_6$ (**1**): C, 30.78; H, 1.29%. Found: C, 30.49; H, 1.63%. IR (cm^{-1}): 3565 s, 3509 bs, 1671 s, 1601 s, 1495 m,1466 s, 1390 vs, 1283 m, 1262 m, 1105 m, 1032 w, 990 s, 908 w, 821 w, 781 m, 669 m, 623 m.

[Ca(BDC-F_4)(MeOH)$_2$]$_n$ (2). The same synthetic procedure as that for **1** was used except that the solvent ethanol was replaced by methanol (6 mL), affording colorless block crystals of **2** in 52% yield (53.1 mg, based on H_2BDC-F_4). Anal. Calcd for $C_{10}H_8CaF_4O_6$ (**2**): C, 35.30; H, 2.37%. Found: C, 34.92; H, 2.41%. IR (cm^{-1}): 3457 bs, 2967 m, 2885 m, 1653 s, 1611 s, 1490 m, 1465 s, 1392 s, 1262 m, 1253 m, 1112 m, 1063 w, 986 s, 886 m, 799 m, 756 s, 673 m, 663 w.

[Ca(BDC-F_4)(H_2O)$_4$]$_n$ (3). Complex **1** (1249.0 mg, 4 mmol) was dissolved in pure water (12 mL). Upon slow evaporation of the solution over five weeks, colorless needle-like crystals of **2** were yielded in 76% yield (949.0 mg, based on **1**). Anal. Calcd. for $C_8H_8CaF_4O_8$ (**2**): C, 27.59; H, 2.32%. Found: C, 27.83; H, 2.68%. IR (cm^{-1}): 3565 s, 3504 bs, 1647 s, 1613 s, 1498 m, 1465 s, 1390 vs, 1261 m, 990 s, 908 w, 782 m, 690 m, 625 m.

Sorption Measurements

The gas sorption isotherms were measured on a ASAP 2020M adsorption equipment. The as-synthesized material was treated by heating at 160 °C for 6 h in a quartz tube under vacuum to remove the solvent molecules prior to measurement.

X-Ray Crystallography

Single-crystal X-ray diffraction measurements of **1–3** were performed on a Bruker APEX II CCD diffractometer at the ambient temperature with Mo Kα radiation (λ = 0.71073 Å). In each case, a semiempirical absorption correction was applied using SADABS, and the program SAINT was used for integration of the diffraction profiles.[15] The structures were solved by the direct methods and refined by the full-matrix least-squares on F^2 using the SHELXTL program.[16] All non-hydrogen atoms were refined anisotropically. C–bound hydrogen atoms were placed in geometrically calculated positions by using a riding model. O–bound hydrogen atoms were localized by difference Fourier maps and refined in subsequent refinement cycles. The details of crystallographic parameters, data collection and refinements for the complexes are listed in Table 1, and selected bond lengths and angles with their estimated standard deviations are listed in Table S1 (ESI†).

Table 1 Crystallography data and details of diffraction experiments for complexes **1–3**.

	1	**2**	**3**
Formula	$C_{32}H_{16}Ca_4F_{16}O_{24}$	$C_{10}H_8CaF_4O_6$	$C_8H_8CaF_4O_8$
M_r	1249.77	340.24	348.22
Crystal system	Tetragonal	Monoclinic	Monoclinic
Space group	$P4_12_12$	$C2/c$	$P2_1/m$
a/Å	14.835(1)	10.950(1)	3.739(1)
b/Å	14.835(1)	17.701(1)	22.568(7)
c /Å	6.785(1)	7.843(1)	6.767(2)
α/°	90	90	90
β/°	90	102.330(1)	93.286(6)
γ/°	90	90	90
V/Å^3	1493.4(2)	1485.0(1)	1049.3(4)
Z	1	4	2
D_c/g cm^{-3}	1.388	1.522	2.028
μ/mm^{-1}	0.478	0.488	0.650
R_{int}	0.0113	0.0358	0.0240
R^a, $R_w{}^b$	0.0525, 0.1287	0.0639, 0.2168	0.0298, 0.0791
GOF on F^2	1.042	1.035	1.067
Flack factor	0.05(1)	–	–

^{a} $R = \Sigma||F_o| - |F_c||/\Sigma|F_o|$. ^{b} $R_w = \Sigma[w(F_o^2 - F_c^2)^2]/\Sigma[w(F_o^2)^2]^{1/2}$.

Results and Discussion

Crystal structures of complexes 1–3

{[Ca_4(BDC-F_4)$_4$(H_2O)$_4$]·4H_2O}$_n$ (1). Single-crystal X-ray diffraction analysis reveals that complex **1** crystallizes in the chiral space group $P4_12_12$ with the absolute structure parameter (flack parameter) being +0.05(1), indicating each individual crystal consists of a single enantiomer.[17] The asymmetric unit of **1** consists of one Ca^{II} center, one BDC-F_4 dianion, one aqua ligand, and two half-occupied independent lattice water molecules. Each Ca^{II} ion is seven-coordinated in a distorted pentagonal-bipyramidal geometry (CaO_7), being defined by six carboxylate oxygen donors from five different BDC-F_4 dianions with the Ca–O distances in the range of 2.335(3) – 2.556(3) Å

and one oxygen atom from one aqua ligand with the Ca–O distance of 2.270(1) Å (Fig. 1a). The BDC-F_4 ligand exhibit two different types of coordination mode with one carboxylate group displaying a μ_2-η^1:η^1-*syn*-*syn*-bridging fashion and the other one displaying a μ_3-η^2:η^2-chelating/bridging mode to connect five Ca^{II} ions. Thus, the CaO_7 pentagonal bipyramid share edges and form a 1D Ca–O–C rods running along the *c* axis (Fig. 1b). Moreover, each rod cross-links four neighboring rods through the perfluorinated benzene rings of BDC-F_4 ligands, generating a 3D rod-packing framework, where the square-shaped channels with a cross-section of *ca.* 14.8 × 14.8 $Å^2$ along the *c*-axis, as indicated in Fig. 1c. Topological analysis revealed that compound **1** can be described as a **sra** net, as defined by the Recticular Chemistry Structure Resource,[18] or a rare binodal 5-connected network (Fig. 1d) with the Schläfli symbol of $\{4^3.6^5.8^2\}\{4^6.6^4\}$, determined using TOPOS.[19] The channel interior is decorated with fluorine groups of BDC-F_4 ligands that make the fluorous pore surface highly polar. Calculation using PLATON[14] suggests that after the removal of all water molecules, the fluorine-lined channels possesses a void volume of 1980.9 $Å^3$ (about 40.0% of the unit-cell volume), which is comparable to that of **FMOF-1**.[20]

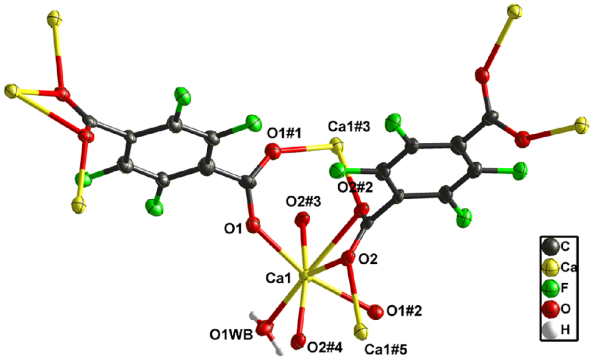

(a)

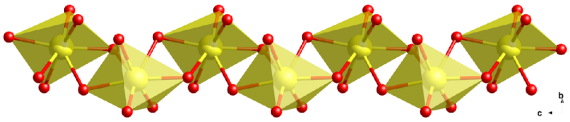

(b)

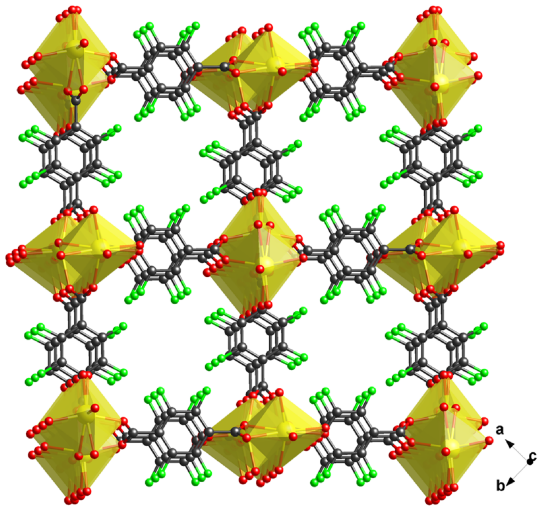

(c)

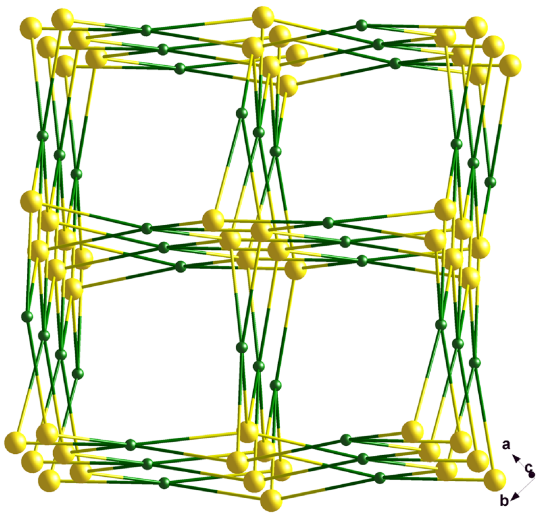

(d)

Fig. 1. Views of **1**: (a) The coordination environment of Ca^{II} and the binding mode of BDC-F_4. Symmetric codes: (1) $-x+1, -y+1, -z+5/2$; (2) $x, y, -z+2$; (3) $-x+1, -y+1, z+1/2$; (4) $-x+1, -y+1, -z+3/2$; (5) $-x+1, -y+1, z-1/2$. (b) Polyhedral representation of the infinite 1D rod SBUs. (c) 3D coordination framework. (d) A schematic representation of the 3D 5-connected network.

Remarkably, the lattice water molecules are included in the fluorine-lined channels, which form a chiral 3D water network via hydrogen bonding with the coexistence of two asymmetric helical arranges of water chains. The water molecules of O2W and O3W and their symmetric ones are arranged in high order to afford a water channel with *M*-helices along [001] (Fig. 2a), with the helical pitch of *c* axis length and the period for each repeating unit of *b* axis length. The average O···O distance in such a water helix is 2.592(1) Å, which is clearly shorter than the sum of their van der Waals radii (r_{vdW} for O = 1.52 Å), revealing the presence of strong noncovalent O···O interaction. Moreover, the O3W water molecules are hydrogen bonded to each other (O···O3 = 2.934 Å) to afford a smaller channel with *P*-helices (right-handed) C4 water chain along the *c* axis (Fig. 2b).[21] Notably, the O3W–O3W$^{\#2}$–O3W angle (109.5°) agrees well with that of the preferred tetrahedral arrangement for ice I_h,[22] which further indicates the similarity between helical C4 water morphology and ice I_h. Such two types of helical water motifs are further combined through O3W molecules to afford a 3D H-bonding network with (10,3)-*a* topology (Fig. 2c and Fig. 2d). To the best of our knowledge, though the symmetric helical water chains have been known,[23] such helical motifs in **1** containing simultaneously asymmetric *M* and *P* helical water in the same lattice are not observed yet. In addition, weak O2W–H2X···F1 (O···F: 2.877 Å and angle: 146.4°) and O3W–H3X···F1 (O···F: 2.940 Å and angle: 119.2°) bonds between the fluorinated host framework and the encapsulated water aggregation are found. Thus, the fluorine groups of the host coordination framework can be considered as the structure directing agent to determine the orientations of helical water arrays and in turn transfer the chirality. The helical water morphologies act as "guest helix" to be fixed within the perfluorinated host framework.

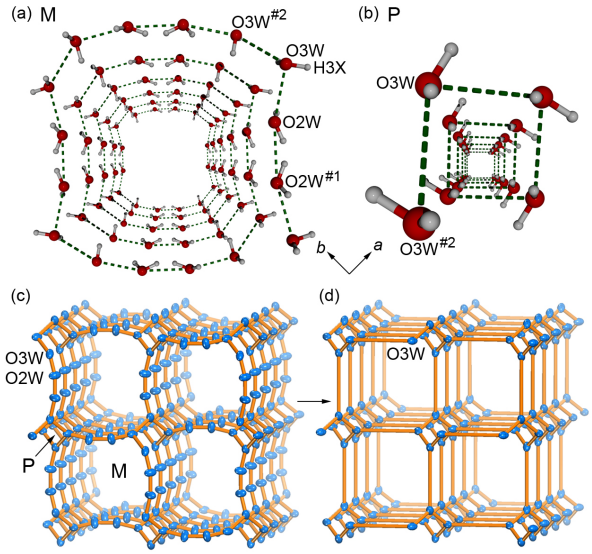

Fig. 2 (a) The 1D *M* helical water chain (O2W···O2W$^{\#1}$ = 2.451 Å; O2W···O3W = 2.521 Å; O3W···O3W$^{\#2}$ = 2.934 Å, symmetry codes: #1 = x, y, $-z$; #2 = $-x+1/2$, $y+1/2$, $z-1/4$); (b) The 1D *P* helical water chain (O3W···O3W$^{\#2}$ = 2.934 Å, symmetry code: #2 = $-x+1/2$, $y+1/2$, $z-1/4$); (c) 3D chiral water net constructed by asymmetric *P* and *M* helical water motifs; (d) The simplified 3D H-bonding water network with (10,3)-*a* topology.

[Ca(BDC-F$_4$)(MeOH)$_2$]$_n$ (2). Complex **2** crystallizes in the centrosymmetric space group *C*2/*c* and contains one Ca^{II} centre, one deprotonated BDC-F$_4$ and two coordinated methanol ligands. The Ca^{II} ion is octahedrally coordinated (CaO$_6$) to four different BDC-F$_4$ ligands with the Ca–O distances of 2.339(4) and 2.457(4) Å and two terminal methanol ligands with the the Ca–O distance of 2.377(4) Å (Fig. 3a). The BDC-F$_4$ ligand is linked to four Ca^{II} ions with each carboxylate group adopting the μ_2-η^1:η^1-*syn-anti*-bridging mode. The CaO$_6$ octahedra are repeated infinitely in the *c* axis, generating a linear Ca–O–C rod (Fig. 3b), which is linked to four neighboring rods by the tetrafluorinated benzene rings of the BDC-F$_4$ to give the 3D framework (Fig. 3c) with the **sra** net topology that is similar to **1**. However, in another way of topological analysis, if each Ca^{II} ion is regarded as a four connected tetrahedral node and each BDC-F$_4$ as a square building block, the resulting 3D structure of **2** can be described as a binodal 4-connected **pts** net with the Schläfli symbol of $\{4^2.8^4\}$ (Fig. 3d). In addition, owing to the existence of obstructive terminal methanol entities that point toward the rhombus-shaped channels, such a 3D framework has very small voids of 84.2 Å^3 (only 5.7% of the unit cell volume) as calculated by PLATON.[14]

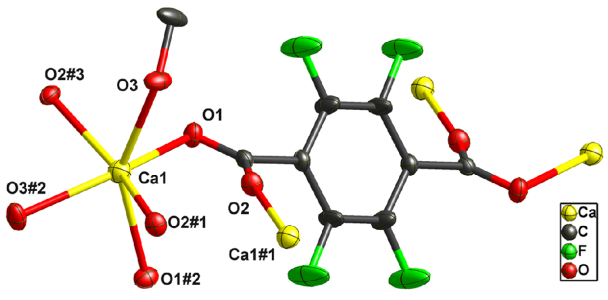

(a)

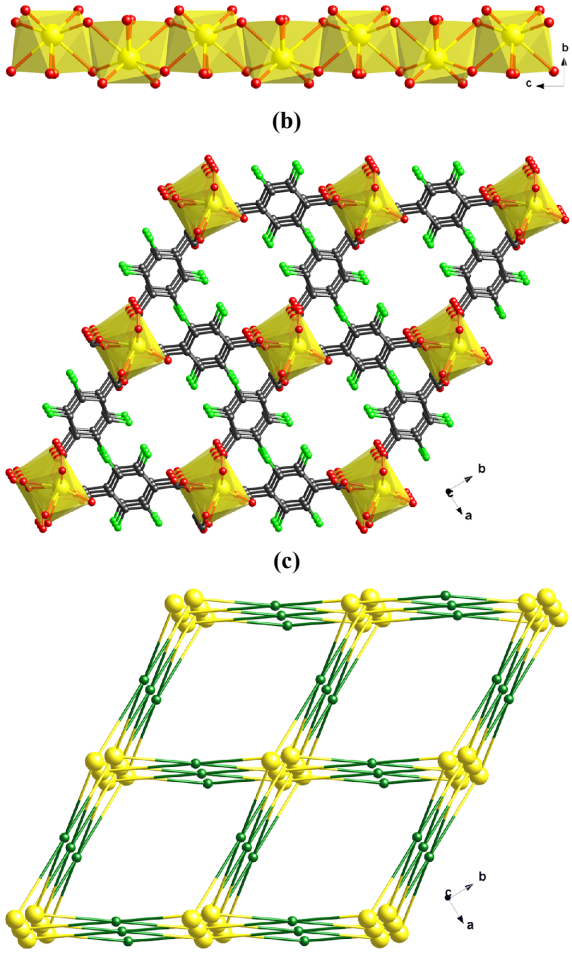

Fig. 3. Views of **2**: (a) The coordination environment of Ca^{II} and the binding mode of BDC-F$_4$. Symmetric codes: (1) $-x+1, -y+1, -z$; (2) $-x+1, y, -z+1/2$; (3) $x, -y+1, z+1/2$. (b) Polyhedral representation of the infinite 1D rod SBUs. (c) 3D coordination framework. (d) A schematic representation of the 3D 4-connected network with **pts** topology.

[Ca(BDC-F$_4$)(H$_2$O)$_4$]$_n$ (3). X-ray structural analysis reveals that **3** crystallizes in the space group $P2_1/m$ and shows a 2-D layer framework, different from the 3D chiral structure of **1**. The asymmetric unit of **3** is composed of one Ca^{II} ion, one BDC-F$_4$ dianion and four aqua ligands. As shown in Fig. 4a, each Ca^{II} center is nine-coordinated by two BDC-F$_4$ ligands and seven water molecules with the Ca–O distance in the range of 2.428(3)–2.598(2) Å. In **3**, the centrosymmetric BDC-F$_4$ ligand adopts the monodentate coordination mode for each carboxylate to bridge two Ca^{II} ions. Two adjacent Ca^{II} ions are linked by three μ_2-O atoms of aqua ligands to construct a 1D [Ca–H$_2$O]$_n$ chain (Fig. 4b). It should be emphasized that polymeric chains of aqua-metal complexes of s-block metal are quite limited. In fact, only several complexes consisting of 1D aqua-metal chain have been reported,[24] where the adjacent metal centers are bridged by two water molecules. Further, the infinite aqua-metal species with the triple μ_2-O aqua bridges are even rare and only found for metal ions such as Na^{I},[25] K^{I},[26] and Sr^{II}.[27] To our knowledge, complex **3**

represents the first example for $[Ca–H_2O]_n$ chain based on triple aqua bridges.

Such 1D $[Ca–H_2O]_n$ motifs are extended by BDC-F_4 spacers to afford a 2D wave-like layer (Fig. 4c), where the adjacent Ca···Ca distances separated by BDC-F_4 and H_2O ligands are 12.563(3) and 3.739(1) Å, respectively. Further investigation of the crystal packing of **3** suggests that the adjacent layers are stacked parallel along the [001] direction, which are interconnected via interlayer O–H···O H-bonding interactions between coordinated water molecules and the uncoordinated carboxylate oxygen atom of BDC-F_4 to realize the final 3D supramolecular architecture.

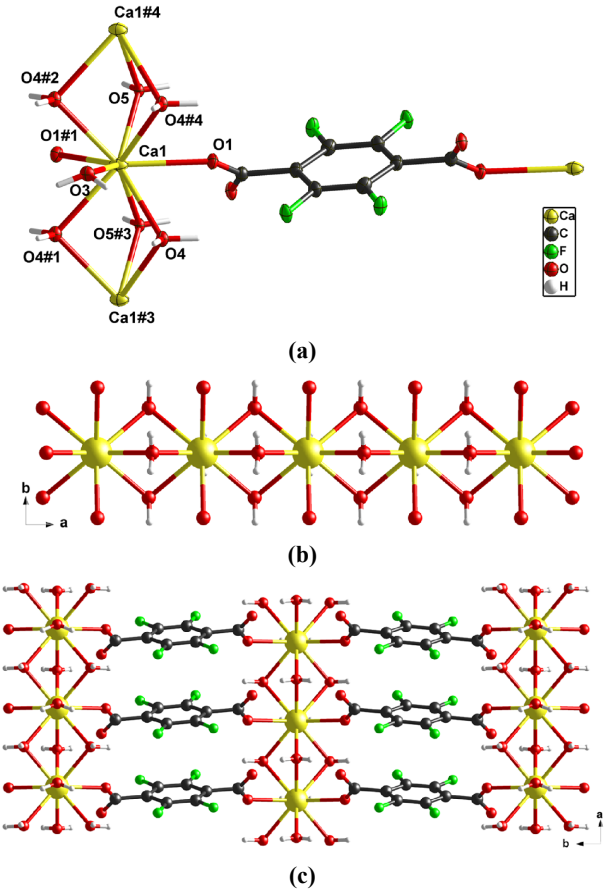

Fig. 4. Views of **3**: (a) The coordination environment of Ca^{II} and the binding mode of BDC-F_4. Symmetric codes: (1) $x, -y + 3/2, z$; (2) $x + 1, -y + 3/2, z$; (3) $x - 1, y, z$; $x + 1, y, z$. (b) The 1D $[Ca–H_2O]_n$ chain based on triple aqua bridges. (c) The 2D layered structure along the *ab* plane.

Solven effect and water-induced structural transformation

It was realized that solvents play an important role in the design and synthesis of coordination networks and supramolecular assemblies. Solvents with different sizes and coordination abilities not only facilitate the crystallization of well-defined molecular architectures, but also trigger physicochemical properties such as adsorption, magnetism, catalysis, and chirality etc.[28] In particular, the solvent-dependent structural assemblies of chiral coordination compounds based on achiral ligands have been recently reported, although they are very rare.[29] Complexes **1** and **2** were synthesized in different solvent systems (DMF/ethanol for **1** and DMF/methanol for **2**) through the facile assembly reaction of an equimolar $Ca^{II}/H_2BDC\text{-}F_4$ mixture at ambient conditions (see Scheme 1). In **1**, the ethanol and DMF are not included in the final crystalline product, and water serves as both the terminal ligand and guest molecules. Notably, guest water molecules are involved in the intermolecular O–H···F hydrogen interactions with the fluorinated host framework, which is responsible for the spontaneous formation of chiral water network. As for **2**, when the solvent system was replaced with a mixture solvent of methanol and DMF, only the coordinated methanol occupies the potential channel space. Moreover, the difference of solvent systems also contributes to the different coordination modes of carboxylate groups, that is, μ_2-η^1:η^1-bridging and μ_3-η^2:η^2-chelating/bridging for **1** (see Scheme 2a), and μ_2-η^1:η^1-*syn*-*anti*-bridging for **2** (see Scheme 2b), respectively. As a result, the different net topologies from binodal 5-connected for **1** to bimodal 4-connected for **2** are observed. Since the only difference for the synthetic process of **1** and **2** is the crystallization medium, illustrating the tuning effect of the solvent on the formation of such chiral or achiral Ca^{II} MOFs based on the achiral ligand $H_2BDC\text{-}F_4$.

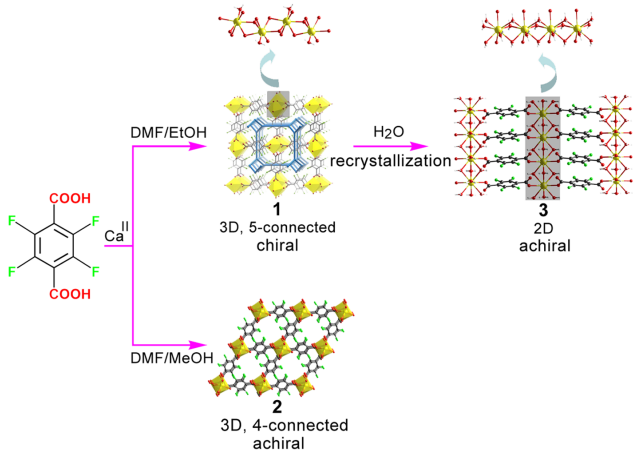

Scheme 1 Summary of the formation of chiral/achiral Ca-MOFs

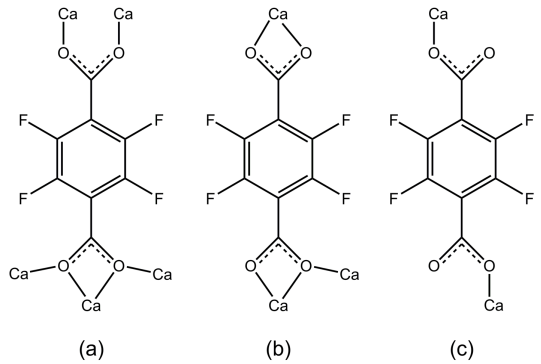

Scheme 2 Coordination modes of BDC-F_4 in **1**–**3**

Interestingly, both **1** and **2** exhibit water solubility and are insoluble in common organic solvents (such as alcohol, chloroform, acetonenitrile and DMF). However, **1** is more highly water-soluble with a solubility of *ca.* 130 mg mL^{-1} than that of **2** with a water solubility of *ca.* 20 mg mL^{-1}. Further, molecular conductivity of water solution of **1** and **2** at room temperature

was determined. The observed values of molecular conductivity for **1** and **2** are 16.27 and 3.52 mS m^2 mol^{-1}, respectively, indicating that **1** should dissociate into ionic metal species and confirm its unusually high solubility. Thus, recrystallization of **1** in aqueous solution may occur readily. Upon slowly evaporating the water solution of **1**, a new Ca^{II} MOF of **3** was successfully achieved. In contrast to **1**, even higher water solubility of *ca.* 180 mg mL^{-1} was observed for **3**, and its value of molecular conductivity reaches 21.52 mS m^2 mol^{-1} at room temperature. On the other hand, it should be pointed out that the procedure of water-induced structural conversion from **1** to **3** is irreversible since complex **3** is almost insoluble in DMF and ethanol.

A further structural comparison between **1** and **3** shows the effect of such water-induced transformation on the final frameworks. In **1**, the seven-coordinated Ca^{II} ion is completed by five BDC-F_4 dianions and one aqua ligand, while the nine-coordinated Ca^{II} center in **3** is surrounded by two BDC-F_4 dianions and seven aqua ligands. In contrast, the BDC-F_4 ligand in **3** shows the monodentate coordination mode (see Scheme 2c) for each carboxylate group. As a consequent, it leads to the generation of 1D $[Ca(COO)_2(H_2O)]_n$ for **1** and $[Ca(COO)_2(H_2O)_4]_n$ for **3**, respectively (see Scheme 1). In addition, the BDC-F_4 ligand displays distinct connectivities in the complexes **1** and **3** presented here (see Scheme 1a for **1** and Scheme 1c for **3**). Based on the above mentioned, the different coordination frameworks of them (3D for **1** and 2D for **3**) were obtained. This result illustrates that the superhydrophilic racemic mixture of chiral crystalline solids for **1** can be converted to an achiral MOF **3** when a large amount of water is introduced. To the best of our knowledge, such a drastic structural transformation for MOFs from 3D chiral to 2D achiral crystals induced by water has not been reported so far.

Stability and gas sorption properties of 1

Thermogravimetric analyses (TGA) of **1**–**3** indicate that solvent molecules were lost in the temperature range 45–160 °C (found 10.61%, calculated 11.52% for **1**), 20–130 °C (found 19.46%, calculated 18.81% for **2**) and 40–160 °C (found 19.73%, calculated 20.67% for **3**), respectively (see Fig. S1). Powder X-ray diffraction (PXRD) measurements for **1**–**3** show that the experimental PXRD patterns match well the corresponding simulated ones obtained from single-crystal diffraction data (see Fig. S2 and Fig. S3). To check the porosity of fluorinated MOF **1**, the fresh sample was soaked with dry acetone and then activated under high vacuum at 160 °C for 6 h to generate the dehydrated framework **1a**. The PXRD pattern of **1a** matches with that of the as-synthesized **1** (Fig. S2, ESI†), indicating that the anhydrous porous framework is maintained after removal the water in 1D channels. Gas adsorption for N_2 and CO_2 at 77 and 195 K, respectively, was further explored for anhydrous porous framework **1a**. Adsorption analysis of N_2 shows negligible uptake, while surprisingly significant uptake is observed for CO_2 (81.1 cm^3 g^{-1} at 195 K) (see Fig. 5). The CO_2 sorption isotherm displays obvious hysteresis arising from the interactions between CO_2 molecules and the host framework. Fitting the Langmuir equation to CO_2 sorption isotherm gives an estimated surface area of 348 m^2 g^{-1}. The selective sorption of CO_2 over N_2 can be primarily attributed to their different electrostatic interactions to the porous surface. For **1a**, besides that the numerous F atoms in the channels are more attractive to CO_2 than other gases for the strong quadrupole–quadrupole interactions,[30] the exposed Ca^{II} ions, stemming from the release of coordinated water molecules, can also result in an electric field interacting with the quadrupole molecule such as CO_2. In addition, the smaller kinetic diameter of CO_2 (*ca.* 3.3 Å) than N_2 (3.64 Å) also enables more adsorbing sites to be accessible in the channels and thus its filling easily.

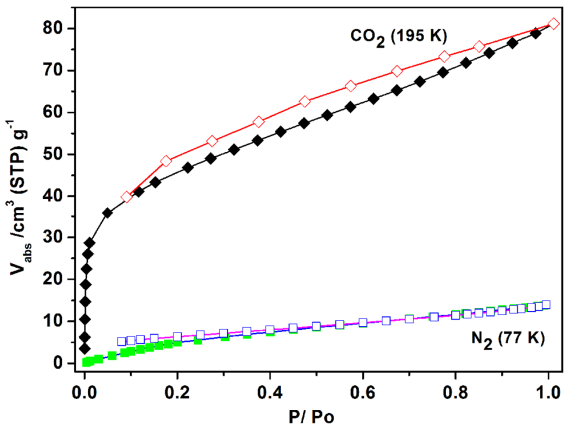

Fig. 5. Gas sorption isotherms of N_2 (77 K) and CO_2 (195 K) for **1a**.

Conclusions

In summary, the construction of 3D chiral and achiral Ca-based MOFs can be realized based on a rigid achiral perfluorinated benzenedicarboxylate in different solvents. The chiral MOF framework hosts an unprecedented 3D chiral water network comprising two distinct helical water units, and this perfluorous MOF also exhibits sorption selectivity of CO_2, which may possess potential applications in the separation of greenhouse gases. Further, the superhydrophilic chiral MOF can act as a precursor to produce a new achiral 2D MOF by recrystallization in water, along with a transformation from chiral to achiral crystals. More efforts on the halogen-induced effect on coordination assemblies of chiral MOFs with achiral halogenated ligands are currently under way.

Acknowledgements

This work was supported by the National Natural Science Foundation of China (21031002, 21101017, 21201026 and 21276029), Jiangsu Key Laboratory of Advanced Catalytic Materials and Technology (BM2012110), the Nature Science Foundation of Jiangsu Province (BK20131142), the Open Foundation of Jiangsu Province Key Laboratory of Fine Petrochemical Technology (KF1105), and Program for Innovation Team Building at Institutions of Higher Education in Chongqing (KJTD201309)

Notes and references

[a] *School of Pectrochemical Engineering, Jiangsu Key Laboratory of Advanced Catalytic Materials and Technology, Changzhou University, Changzhou 213164, P. R. China. E-mail: chenqunjpu@yahoo.com.*
[b] *School of Chemical Engineering, Nanjing University of Science & Technology, Nanjing 210094, P. R. China.*
[c] *College of Chemistry, Chongqing Normal University, Chongqing 401331, P. R. China.*
[d] *College of Chemistry, Tianjin Key Laboratory of Structure and Performance for Functional Molecules, MOE Key Laboratory of Inorganic-Organic Hybrid Functional Material Chemistry, Tianjin Normal University, Tianjin 300387, P. R. China. E-mail: dumiao@public.tpt.tj.cn (M. D.)*

† Electronic Supplementary Information (ESI) available: selected bond lenghths and angles, TGA curves for **1**–**3**, powder X-ray diffraction patterns, and crystallographic data (in CIF format). CCDC reference numbers 1003028–1003030 are for **1**–**3**, respectively. See DOI: 10.1039/b000000x/.

1 (*a*) J. R. Li, J. Sculley and H. C. Zhou, *Chem. Rev.*, 2012, **112**, 869; (*b*) M. O'Keeffe and O. M. Yaghi, *Chem. Rev.*, 2012, **112**, 675; (*c*) C. Wang, T. Zhang and W. B. Lin, *Chem. Rev.*, 2012, **112**, 1084; (*d*) W. Zhang and R. G. Xiong, *Chem. Rev.*, 2012, **112**, 1163; (*e*) Y. J. Cui, Y. F. Yue, G. D. Qian and B. L. Chen, *Chem. Rev.*, 2012, **112**, 1126.
2 (*a*) T. Uemura, N. Yanai and S. Kitagawa, *Chem. Soc. Rev.*, 2009, **38**, 1228; (*b*) Z. Wang and S. M. Cohen, *Chem. Soc. Rev.*, 2009, **38**, 1315; (*c*) J. Lee, O. K. Farha, J. Roberts, K. A. Scheidt, S. T. Nguyen and J. T. Hupp, *Chem. Soc. Rev.*, 2009, **38**, 1450.
3 (*a*) D. Bradshaw, J. B. Claridge, E. J. Cussen, T. J. Prior and M. J. Rosseinsky, *Acc. Chem. Res.*, 2005, **38**, 273; (*b*) B. Kesanli and W. B. Lin, *Coord. Chem. Rev.*, 2003, **246**, 305.
4 S. C. Sahoo, T. Kundu and R. Banerjee, *J. Am. Chem. Soc.*, 2011, **133**, 17950.
5 (*a*) L. J. Barbour, G. W. Orr and J. L. Atwood, *Nature*, 1998, **393**, 671; (*b*) M. Zuhayra, W. U. Kampen, E. Henze, Z. Soti, L. Zsolnai, G. Huttner and F. Oberdorfer, *J. Am. Chem. Soc.*, 2006, **128**, 424; (*c*) B. Q. Ma, H. L. Sun and S. Gao, *Chem. Commun.*, 2005, **18**, 2336.
6 (*a*) S. Pal, N. B. Sankaran and A. Samanta, *Angew. Chem., Int. Ed.*, 2003, **42**, 1741; (*b*) M. H. Mir, L. Wang, M. W. Wong and J. J. Vittal, *Chem. Commun.*, 2009, **30**, 2336.
7 (*a*) B. Q. Ma, H. L. Sun and S. Gao, *Angew. Chem., Int. Ed.*, 2004, **43**, 1374; (*b*) Q. G. Meng, S. T. Yan, G. Q. Kong, X. L. Yang and C. D. Wu, *CrystEngComm*, 2010, **12**, 688.
8 (*a*) R. Carballo, B. Covelo, C. Lodeiro and E. M. Vázquez-López, *CrystEngComm*, 2005, **7**, 294; (*b*) Y. G. Huang, Y. Q. Gong, F. L. Jiang, D. Q. Yuan, M. Y. Wu, Q. Gao, W. Wei and M. C. Hong, *Cryst. Growth Des.*, 2007, **7**, 1385.
9 B. L. Wu, S. Wang, R. Y. Wang, J. X. Xu, D. Q. Yuan and H. W. Hou, *Cryst. Growth Des.*, 2013, **13**, 518.
10 K. Bhattacharyya, *Chem. Commun.*, 2008, **25**, 2848.
11 (*a*) B. Sreenivasulu and J. J. Vittal, *Angew. Chem., Int. Ed.*, 2004, **43**, 5769; (*b*) B. Zhao, P. Cheng, X. Y. Chen, C. Cheng, W. Shi, D. Z. Liao, S. P. Yan and Z. H. Jiang, *J. Am. Chem. Soc.*, 2004, **126**, 3012.
12 B. K. Saha and A. Nangia, *Chem. Commun.*, 2005, **24**, 3024.
13 (*a*) S. C. Chen, Z. H. Zhang, Q. Chen, L. Q. Wang, J. Xu, M. Y. He, M. Du, X. P. Yang and R. A. Jones, *Chem. Commun.*, 2013, **49**, 1270; (*b*) Z. H. Zhang, S. C. Chen, M. Y. He, C. Li, Q. Chen and M. Du, *Cryst. Growth Des.*, 2011, **11**, 5171.
14 (a) A. L. Spek, *J. Appl. Crystallogr.*, 2003, **36**, 7; (b) A. L. Spek, *PLATON*, *A Multipurpose Crystallographic Tool*, Utrecht University, Utrecht, The Netherlands, 2002.
15 Bruker AXS, *SAINT Software Reference Manual*, Madison, WI, 1998.
16 G. M. Sheldrick, S*HELXTL NT Version 5.1. Program for Solution and Refinement of Crystal Structures*, University of Göttingen, Germany, 1997.
17 H. D. Flack, *Acta Crytallogr., Sect. A*, 1983, **39**, 876.
18 M. O'Keeffe, M. A. Peskov, S. J. Ramsden and O. M. Yaghi, *Acc. Chem. Res.*, 2008, **41**, 1782, and the Reticular Chemistry Structure Resource website at http://rcsr.anu.edu.au.
19 V. A. Blatov, A. P. Shevchenko and V. N. Serezhkin, *J. Appl. Crystallogr.*, 2000, **33**, 1193, see also http://www.topos.ssu.samara.ru.
20 C. Yang, X. Wang and M. A. Omary, *J. Am. Chem. Soc.*, 2007, **129**, 15454.
21 L. Infantes, J. Chisholm and S. Motherwell, *CrystEngComm*, 2003, **5**, 480.
22 The value is taken from the data at 200 K. D. Eisenberg and W. Kauzmann, *The Structure and Properties of Water*, Oxford University Press, Oxford, 1969.
23 (*a*) X.-Y. Duan, X. Cheng, J.-G. Lin, S.-Q. Zang, Y.-Z. Li, C.-J. Zhu and Q.-J. Meng, *CrystEngComm*, 2008, **10**, 706; (*b*) K.-L. Zhang, C.-T. Hou, J.-J. Song, Y. Deng, L. Li, S. W. Ng and G.-W. Diao, *CrystEngComm*, 2012, **14**, 590.
24 (a) E. Elacqua, P. Kaushik, R. H. Groeneman, J. C. Sumrak, D.-K. Bučar and L. R. MacGillivray, *Angew. Chem., Int. Ed.*, 2012, **51**, 1037; (b) T. L. Kinnibrugh, N. Garcia and A. Clearfield, *J. Solid State Chem.*, 2012, **187**, 149; (c) T. E. Clark, A. Martin, M. Makha, A. N. Sobolev, D. Su, H. W. Rohrs, M. L. Gross and C. L. Raston, *Cryst. Growth Des.*, 2010, **10**, 3211.
25 S. G. Baca, H. Adams, C. S. Grange, A. P. Smith, I. Sazanovich and M. D. Ward, *Inorg. Chem.*, 2007, **46**, 9779.
26 B. F. Abrahams, C. T. Abrahams, M. G. Haywood, T. A. Hudson, B. Moubaraki, K. S. Murray and R. Robson, *Dalton Trans.*, 2012, **41**, 4091.
27 J.-B. Arlin, A. J. Florence, A. Johnston, A. R. Kennedy, G. J. Miller and K. Patterson, B. F. Abrahams, C. T. Abrahams, M. G. Haywood, T. A. Hudson, B. Moubaraki, K. S. Murray and R. Robson, *Cryst. Growth Des.*, 2011, **11**, 1318.
28 (a) C. P. Li and M. Du, *Chem. Commun*., 2011, **47**, 5958; (b) X. Chen, S. B. Qiao, D. Liu, J. P. Lang, Y. Zhang, C. Xu and S. L. Ma, *CrystEngComm*, 2010, **12**, 1610; (c) Y. Chen, H. X. Li, D. Liu, L. L. Liu, N. Y. Li, H. Y. Ye, Y. Zhang and J. P. Lang, *Cryst. Growth Des.*, 2008, **8**, 3810.
29 (a) X. D. Chen, M. Du and T. C. W. Mak, *Chem. Commun*., 2005, **35**, 4417; (b) T. Ezuhara, K. Endo and Y. Aoyama, *J. Am. Chem. Soc*., 1999, **121**, 3279.
30 P. Pachfule, Y. Chen, J. Jiang and R. Banerjee, *Chem.–Eur. J*., 2012, **18**, 688.